Using Type Ia Supernovae and Galaxy Clusters to Constrain Cosmology

A thesis submitted in partial fulfillment of the requirement
for the degree of Bachelor of Science with Honors in
Physics from the College of William and Mary in Virginia,

by

Lukas D. Osborne

Accepted for _____
(Honors)

_____
Advisor: Dr. Joshua Erlich

_____
Dr. William Kossler

_____
Dr. Carl Carlson

_____
Dr. Nahum Zobin

Williamsburg, Virginia
April 23, 2008

Abstract

The basic methods of statistical analysis used in cosmology surveys are studied through a review of observations made by the Supernovae Legacy Survey. Theoretical predictions for the apparent magnitude of Type Ia supernovae are compared to observed magnitudes in order to place constraints on a (Ω_m, w_Λ) cosmology. Analytical models describing structure formation, and the comparison of astronomical observation to mass, are used to predict number counts for galaxy clusters. Through comparison of these predictions, and observations from the ROSAT 400 Square Degree data set, constraints on a (Ω_m, w_Λ) cosmology are made. The constraints developed by the supernovae and structure formation approaches are then superimposed to generate a global fit. Throughout this process, the best fit values obtained for the free parameters are compared with values from the WMAP five year results.

Acknowledgements

The author would like to thank Dr. Joshua Erlich for his patience and guidance during the time in which this research was conducted. Thanks is also owed to Brian Glover whose help and advice at many stages was invaluable. Additionally, appreciation is extended to Dr. Carl Carlson and Dr. Nahum Zobin for graciously serving on the honors committee.

Contents

1 Introduction

In the past few decades, advances in astrophysical and cosmological observations have marked the beginning of the era of precision cosmology. Data sets from a variety of studies have placed strong constraints on many features of our universe. Some of these data sets include studies of the (*i*) cosmic microwave background, (*ii*) luminosity-redshift curves of Type Ia supernovae, and (*iii*) large scale structure formation:

(*i*) The standard model of cosmology is described by the inflationary Big Bang where the current universe evolved from a hot, dense state by way of a period of exponential expansion. As the universe expanded, the temperature of the primordial plasma dropped, allowing photons to decouple from matter during a period called recombination. Today the temperature fluctuations of these photons are observed as the cosmic microwave background (CMB) and are measured by satellites such as the Wilkinson Microwave Anisotropy Probe (WMAP) [1].

(*ii*) In the last decade, the study of luminosity-redshift curves of Type Ia supernovae (SNe) provided the first, direct evidence of the accelerated expansion of the universe [2]. This acceleration revealed the existence of an unknown energy density with negative pressure, which we refer to as dark energy. Discovering the nature of dark energy is a primary focus in modern cosmology. The details of Ia SNe and their role in cosmology is included in Section 3.

(*iii*) Small density fluctuations in the primordial plasma were enhanced during recombination and cosmic expansion. These regions of overdensity act as the seed for large scale structure - another important probe to cosmology. The evolution of structure depends on the expansion history of the universe and is therefore sensitive to its components. Since galaxy clusters are the largest known objects in the universe, and in the hierarchy of structure formation, the last to form, they can be used to study the composition of the universe. A current challenge for cluster surveys lies in accurately describing the relationship between astrophysical measurements and mass [3]. Details of how the Press-Schechter formalism [4]

can be used to predict number counts of virialized objects such as clusters is discussed in Section 4.

Observations of the CMB taken from WMAP have been very successful in placing constraints on many cosmological parameters which characterize the composition of the universe. For example, from the WMAP five-year data set [1], the geometry of the universe is shown to be nearly flat and its present-day age is 13.69 ± 0.13 Gyr (one standard deviation errors). When combined with other data sets, the constraints on these parameters are more stringent. Measurements from WMAP and Type Ia SNe, for instance, can sometimes place better constraints on parameters than either can do alone (*e.g.*, Ω_Λ and w_Λ space [1]). Two parameters of particular interest in current cosmological initiatives are the total matter density Ω_m and the dark energy equation of state w_Λ. The importance of these parameters is discussed in the following (more detail is given in Section 2). For a flat cosmology, the total energy density of the universe is given by $\Omega_m + \Omega_\Lambda = 1$, where Ω_Λ is the energy density associated with dark energy. Therefore, knowledge of Ω_m provides information describing the energy budget of the universe. The equation of state parameter for dark energy relates its pressure p and density ρ through $p = w_\Lambda \rho$. Since the acceleration of the universe depends on the precise value of w_Λ, knowledge of this parameter sheds light on the mysterious nature of dark energy and the expansion of the universe.

The purpose of this paper is two fold. First, the basic methods of statistical analysis used in cosmology surveys will be studied through a review of observations made by the Supernovae Legacy Survey [5]. Theoretical predictions for the apparent magnitude (*i.e.* brightness, see Section 3) of supernovae will be compared to observed magnitudes in order to place constraints on the parameters Ω_m and w_Λ. Second, analytical models describing structure formation, and the comparison of astronomical observation to mass, will be used to predict number counts for galaxy clusters. Although the most sophisticated studies in structure formation employ elaborate numerical simulations, analytical models are useful in understanding the underlying physics and thus serve as important tools [6, 7, 8, 9]. Through

comparison of theoretical predictions and observations from the ROSAT 400 Square Degree data set [10], constraints on a (Ω_m, w_Λ) cosmology will be made. The constraints developed by the supernovae and structure formation approaches will then be superimposed on one another to generate a global fit. Throughout this process, the best fit values obtained for these parameters will be compared with values from the WMAP five year results.

2 A Brief Background to Cosmology

In this section, an overview of basic principles and formulae involved in the study of cosmology will be introduced. Although a rigorous review of general relativity was outside the scope of this study, certain aspects of the theory are mentioned to provide a basis for what follows.

Cosmic inflation in the early universe justifies the use of the cosmological principle, which states that on very large distance scales, our universe is homogeneous and isotropic (*i.e.* no preference is given to any specific location or direction). Taken together, these features constitute the basis for the study of physical cosmology. The spacetime interval which describes events $(t,\ r,\ \theta,\ \phi)$ and $(t\ +\ dt,\ r\ +\ dr,\ \theta\ +\ d\theta,\ \phi\ +\ d\phi)$, in such a homogeneous and isotropic space, is known as the Robertson-Walker (RW) metric:

$$ds^2 = -c^2dt^2 + R_0^2a^2(t)\left(\frac{dr^2}{1-kr^2} + r^2d\theta^2 + r^2\sin^2\theta d\phi^2\right). \tag{1}$$

In this expression, the parameter R_0 is related to the absolute size of the universe and factor of k can represent open, closed, or flat universes with chosen values of -1, +1, or 0. The time variable t found in the metric is the cosmological proper time, *i.e.* the time elapsed since the big bang, measured by an observer who sees space expand uniformly. In addition, the spatial variables $(r,\ \theta,\ \phi)$ are the comoving coordinates. These coordinates are assigned to objects that move along with the Hubble flow and are time independent.

The RW metric also accounts for distances expanding (or contracting) as time evolves through the dimensionless scale factor $a(t)$. The scale factor is related to the cosmological

redshift z by

$$a = \frac{1}{1+z}, \tag{2}$$

where we set the scale factor at the present time to be $a(\text{today}) = 1$ so that the $z(\text{today}) = 0$. As a review, the redshift of a light source can also be expressed in terms of its received and emitted wavelengths through

$$1 + z = \frac{\lambda_{received}}{\lambda_{emitted}}. \tag{3}$$

It is important to note that the cosmological redshift of a light source is not due to the relative motion of the object compared to the observer. Instead the redshift is caused by the expansion of space through which light is traveling. Therefore, in the context of an expanding universe, redshift measurements naturally provide a timeline of cosmological evolution (*i.e.* different values of z correspond to observations of different points in time). As a result, cosmology studies often use redshift measurements as a surrogate for time.

The Robertson-Walker metric can be used to solve Einstein's field equations under the assumption that sources of matter and energy behave as perfect fluids. These fluids can be described by a linear equation of state $p_i = w_i \rho_i$ where the pressure p_i and energy density ρ_i are related by the equation of state parameter w_i. The solution to Einstein's equations comes in the form of a differential equation for the scale factor $a(t)$:

$$\left(\frac{\dot{a}}{a}\right)^2 = H^2 = \frac{8\pi G}{3c^2} \sum_i \rho_i - \frac{kc^2}{a^2 R_0^2}. \tag{4}$$

Following common practice, the dimensionless energy density parameter

$$\Omega_i = \frac{8\pi G}{3c^2 H^2} \rho_i \tag{5}$$

is introduced, so that we can define[1]

[1]Note that we assume that the density parameters in equation (6) and (7) refer to present-day values. In theory, they evolve with the expansion of the universe since they depend on H, and therefore $a(t)$.

$$\Omega_m \equiv \frac{8\pi G}{3c^2H^2}\rho_m,\ \Omega_\Lambda \equiv \frac{8\pi G}{3c^2H^2}\rho_\Lambda,\ \Omega_{curv.} \equiv -\frac{kc^2}{a^2R_0^2H^2}. \tag{6}$$

This allows us to rewrite equation (5) in the compact form:

$$\Omega_m + \Omega_\Lambda + \Omega_{curv.} = 1. \tag{7}$$

Formulation of this expression is useful for describing the energy budget of the universe. For the purposes of this paper, we assume that the curvature of the universe is flat, thus, $k = 0$ and $\Omega_{curv.} = 0$. This assumption is well motivated by many studies, including the five year WMAP results [1]. We also assume that the subscript Λ refers to a dark energy contribution with negative pressure. The equation of state parameter for this contribution is w_Λ, where $w_\Lambda = -1$ refers to the special case of dark energy taking the form of the cosmological constant. In addition, Ω_m denotes the total matter density of the universe which we assume includes baryonic matter and non-baryonic, cold dark matter (CDM). This matter density can be described by a pressureless dust with equation of state parameter $w_m = 0$. In order to compare with findings from this study, we will use values from the five-year WMAP results as a reference. Using WMAP results alone, the energy budget is found to be dominated by a dark energy contribution, $\Omega_\Lambda = 0.742 \pm 0.030$ [3]. With the assumption of a flat universe, $\Omega_m + \Omega_\Lambda = 1$, we take the total matter density to be $\Omega_m = 0.26$. Since the equation of state parameter for dark energy is not well constrained by WMAP data alone [3], measurements found within this study will be compared to the cosmological constant, $w_\Lambda = -1$.

At this point, it is worthwhile to explain the consequences for certain values of w_Λ. By studying the deceleration parameter, defined as $q(a) = -\ddot{a}a/(\dot{a}^2)$, it can be shown that for $w_\Lambda < -\frac{1}{3(1-\Omega_m)}$, the universe engages in a current period of accelerating expansion. The reason for this is that in general relativity pressure contributes to the gravitational field of a substance, just as mass density does. As a result, positive pressure tends to add to gravitational attraction and negative pressure creates a gravitational repulsion. At

the cosmological scale, the gravitational repulsion caused by the negative pressure of dark energy outweighs any gravitational attraction, and the expansion of the universe accelerates. As the value of w_Λ decreases (beyond the acceleration limit), the negative pressure of dark energy increases as does the gravitational repulsion. The cosmological constant, $w_\Lambda = -1$, corresponds to a expansion which will accelerate exponentially at some point. For $w_\Lambda < -1$, the expansion will eventually accelerate faster than exponentially and may lead to the condition known as the Big Rip. Within this hypothesis, all structure in the universe would be pulled apart as a result of this extreme expansion at some point in the future. The point at which the universe experiences these expansions depends on the composition of the universe.

In continuing with our formulation, each perfect fluid modeled by general relativity has an expression for the conservation of energy:

$$\dot{\rho_i} + 3(\rho_i + p_i)H = 0. \tag{8}$$

This equation can be integrated with respect to time to give:

$$\rho_i = \rho_{0i}(1+z)^{3(1+w_i)}. \tag{9}$$

With equations (6) and (9), the Friedmann equation, equation (4), can be written as

$$H^2(z) = H_0^2(1+z)^2\left[1 + \sum_i \Omega_i((1+z)^{1+3w_i} - 1)\right] \tag{10}$$

where $H_0 = 100h$ km/s/Mpc is the present-day value of the Hubble parameter for $h = 0.732^{+0.031}_{-0.032}$ [11]. The errors correspond to the 68% confidence level.

A principal application of the theory developed so far will be to describe the location of distant light sources. If a photon is assumed to travel radially outward from a source, the θ and ϕ coordinates remain constant so that $d\theta = 0$ and $d\phi = 0$. Making the appropriate substitutions into the RW metric, and noting that photons are known to follow null geodesics ($ds^2 = 0$), we have:

$$\frac{c^2 dt^2}{R_0^2 a^2(t)} = \frac{dr^2}{1 - kr^2}. \tag{11}$$

From here, using equations (2) and (4), we can integrate equation (11) to obtain:

$$\int_0^{r_s} \frac{dr}{\sqrt{1 - kr^2}} = \int_0^{z_s} \frac{cdz}{R_0 H(z)} \tag{12}$$

Substituting $H(z)$ from equation (10) into the right hand side of equation (12) and solving for r_s produces an expression for the comoving distance of a source in terms of its redshift z_s, given by:

$$r_s(z_s) = \frac{c}{R_0 H_0} \int_0^{z_s} \frac{dz}{(1+z)\sqrt{1 + \sum_i \Omega_i [(1+z)^{1+3w_i} - 1]}}. \tag{13}$$

The form of this expression is specific to a flat universe. It is worthwhile to mention that the z found inside the integral of equation (13) is an integration redshift variable. From this point forward, we will relabel z_s as z.

In practice, a significant use of the comoving distance $r_s(z)$ (also called the cosmological proper distance) is in the formulation of the luminosity distance of an object. As a prerequisite, consider the relationship between the radiant flux (F) and the luminosity (L) of a source through:

$$F = \frac{L}{4\pi d^2} \tag{14}$$

where d is the proper distance. This formula is effectively an inverse square law for light in a static Euclidean universe. It is useful in creating a function that depends on the luminosity distance d_L:

$$L = 4\pi (d_L)^2 F. \tag{15}$$

The luminosity distance is an extrapolated distance to an object provided a known intrinsic luminosity and a measured flux. This distance measure is widely implemented in cosmo-

logical studies that use standard candles (See Section 3 for a description of Type Ia SNe as standard candles).

To account for the expansion of the universe, the proper distance d has been replaced by the comoving distance r_s scaled by R_0 (the parameter related to the absolute size of the universe). In addition, two factors of $(1 + z)$ are included to account for photons losing energy through redshift and to incorporate the difference in time intervals during their trajectories. The result of these considerations comes in the form of the following expression for the luminosity:

$$L = 4\pi(R_0(1 + z)r_s(z))^2 F. \tag{16}$$

The luminosity distance can be read off as $d_L = R_0(1 + z)r_s(z)$. From equation (13), we can see that the comoving distance r_s, and hence the luminosity distance, is a function of a specified cosmology described in terms of its energy density and equation of state parameters. This dependance will be of great use as we study Type Ia SNe and galaxy clusters and constrain (Ω_m, w_Λ) cosmologies.

3 Type Ia Supernovae

3.1 Type Ia Supernovae and their role in Cosmology

The standard model for Type Ia supernovae (SNe) creation involves the violent explosion of a white dwarf in a binary star system. Although the exact mechanism behind the explosion is not entirely clear, certain steps do occur which allow us to form a general picture of the event. The white dwarf accretes mass from the companion star until it saturates the Chandrasekhar limit of 1.4 solar masses. At this point, the quantum degeneracy pressure, which initially supports the star, is no longer able to negate the gravitational effects of its own weight. This results in the collapse and explosion of the white dwarf.

A principal application of Type Ia supernovae in cosmological studies is in their use as standard candles. Due to the physical limitations placed on the mass of white dwarfs by

the Chandrasekhar limit, the intrinsic luminosities of Type Ia supernovae throughout the universe are comparable to one another. However, by itself, this feature would not make Type Ia supernovae particularly useful as cosmological standards, since at great distances, fluctuations in apparent luminosity prove to be too large [12]. Fortunately, a clear relationship exists between the intrinsic luminosity of a Type Ia supernovae and the rate of decline in their light curve (*i.e.* a curve that describes luminosity as a function of time). Via the Phillips curve, the intrinsic luminosity of an individual Type Ia supernovae can be found by measuring the time-width of its light curve [12]. Then, with both the intrinsic luminosity and the measured flux, the distance to the supernovae can be computed by equation (16).

In practice, luminous object such as SNe are characterized by an apparent magnitude, defined as:

$$m = m_0 + 5 \log_{10} \left(\frac{H_0 d_L}{c} \right), \tag{17}$$

where m_0 is a magnitude parameter fit to data (sometimes referred to as the absolute magnitude). By convention, the lower the magnitude, the more luminous the object. Notice that the theoretical magnitude m is a function of the luminosity distance d_L, and as argued earlier, it is also a function of a specified cosmology.

3.2 Type Ia Supernovae Data from the Supernova Legacy Survey and Statistical Analysis

This study made use of data collected from the first year of the five year Supernova Legacy Survey (SNLS) [5]. Within the survey, 115 supernovae with redshift $z < 1$ were discovered. Two essential components comprised the observational efforts of the SNLS: an imaging survey to detect SNe and record their light curves, and a spectroscopic program to confirm the samples and measure their redshift [5]. The observed magnitude $\mu_B(z)$ as a function of the recorded redshift for each supernovae event is shown by a Hubble diagram in Figure 1. The relationship between magnitude and redshift, or effectively luminosity distance and

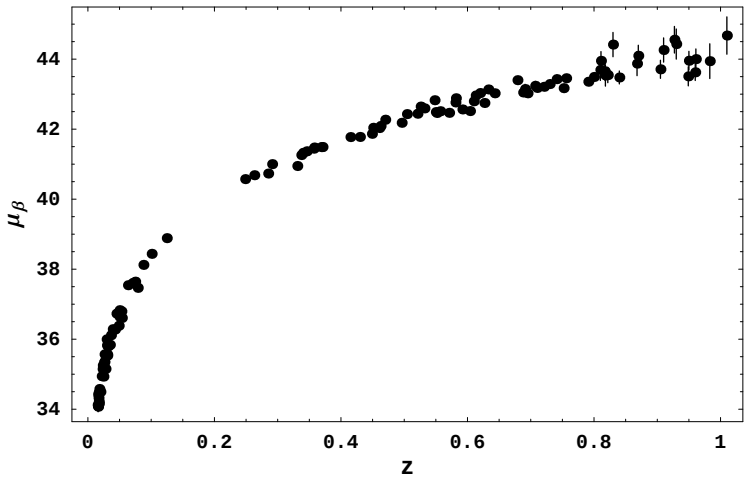

Figure 1: The observed magnitude, including errors, as a function of redshift is shown for 115 Type Ia supernovae from the five year Supernovae Legacy Survey.

redshift, is the most direct evidence for a dark energy component to our universe. The accelerated expansion of space, caused by this dark energy component, leads to the high redshift of emitted photons. The increase in wavelength implies that the photons lose energy was they travel astronomical distances. This translates into a decrease in luminosity and apparent magnitude.

The theoretical machinery behind SNe magnitudes can be used to determine the significance of cosmological models through a χ^2 statistical analysis and the method of least squares. The χ^2 function, for N measurements, takes the general form:

$$\chi^2 = \sum_{i=1}^{N} \frac{(\theta_m^i - \theta_{th}^i)^2}{\sigma_i^2} \tag{18}$$

where θ_m^i and θ_{th}^i represent observed and theoretical values and σ_i denotes the errors. The equation for χ^2 becomes a function of whatever variables the theoretical values depends on. By minimizing χ^2 with respect to these variables, a best fit (for the variables) and associated χ^2_{min} value is obtained. The agreement between observed and theoretical values is deemed reasonable when the χ^2_{min} value is roughly equal to the number of degrees of freedom n_d, defined as the number of measurements minus the number of fitted variables.

In the context of SNe, a χ^2 function can be constructed using the theoretical magnitude m given by equation (17) and the observed magnitudes $\mu_B(z)$ from the SNLS [5]:

$$\chi^2 = \sum_{objects} \frac{(\mu_B - 5\log_{10}(d_L(z)) - m_0)^2}{\sigma^2(\mu_B) + \sigma_{int}^2}. \tag{19}$$

In this equation, the error term consists of two parts: the spread in the observed magnitudes $\sigma^2(\mu_B)$, and the dispersion associated with calculation of the intrinsic luminosity of a supernovae, cited as $\sigma_{int} = 0.13$ [5]. These uncertainties are combined in quadrature to avoid overlap of the individual errors. Careful consideration of the equation (19) leads one to notice that $d_L(z)$ is also a function of a specified cosmology. Assuming a flat universe and setting $w_\Lambda = -1$, χ^2 was initially minimized with respect to m_0 and Ω_m to determine the value of the absolute magnitude (m_0), shared by all SNe. The use of the cosmological constant is reasonable since discrepancies between it and the actual value (for a dark energy contribution) are unlikely to significantly affect the outcome of m_0. When the minimization is computed, $(m_0, \Omega_m) = (43.2, 0.263)$ and $\chi^2_{min} = 112$. This qualifies as acceptable given $n_d = 115 - 2 = 113$. This best fit value for Ω_m is consistent with the SNLS result, $\Omega_m = 0.263 \pm 0.042$, for a cosmological constant contribution ($w_\Lambda = -1$) [5].

With the value of m_0 in hand, χ^2 is then minimized with respect to Ω_m and w_Λ to find a best fit value of $(\Omega_m, w_\Lambda) = (0.285, -1.05)$ corresponding with $\chi^2_{min} = 112$. Again, this is a reasonable result under χ^2 analysis given $n_d = 115$ in this case as well. The best fit value for Ω_m is slightly off the the five year WMAP result, $\Omega_m = 0.26$. A confidence plot can be constructed to view the most probable regions of the (Ω_m, w_Λ) space. To do so, the p-value of the predicted magnitude (theoretical) is defined as:

$$p = \int_{\triangle\chi_0^2}^{\infty} f(\tilde{z}; n_d) dz \tag{20}$$

where $\triangle\chi^2 \equiv \chi^2(x_i) - \chi^2_{min}$ for fitted parameters x_i, in this case (Ω_m, w_Λ). The function $f(\tilde{z}; n_d)$ is the probability density function of a given distribution. For the current analysis, our χ^2 function follows the χ^2 distribution, which is defined as:

$$f(\tilde{z}; n_d) = \frac{\tilde{z}^{n_d/2-1} \exp^{-\tilde{z}/2}}{2^{n_d/2}\Gamma(n_d/2)}. \tag{21}$$

The confidence plots are created by drawing contours of $1-p$ for $\tilde{z} = \triangle\chi^2$. If we assume the theoretical machinery behind SNe magnitudes is correct, these $1-p$ contours represent lines of equal probability that the fitted parameters's true values lie with the enclosed region. This procedure is carried out in (Ω_m, w_Λ) parameter space for $\triangle\chi_0^2$ values corresponding to confidence levels of 68%, 80%, 90% and 95%. The confidence plot is shown in Figure 2.

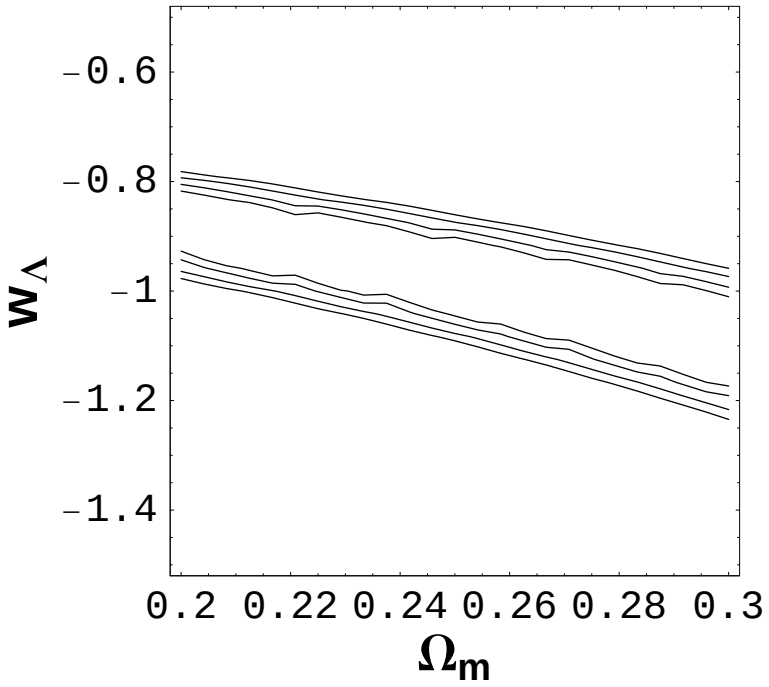

Figure 2: A confidence plot in parameter space from the supernovae data set. The lines represent 68%, 80%, 90%, and 95% confidence regions. The best fit is $(\Omega_m, w_\Lambda) = (0.285, -1.05)$.

By tracing the center of the plot to each axis, the best fit values, achieved by minimizing the χ^2 function, are reobtained. The usefulness of such a confidence plot described here resides in its ability to effectively constrain parameters. The degree to which the parameters are constrained can be improved by supplying additional samples to the data set, superimposing

complementary confidence regions from other sources of data, or statistically combining data sets.

4 Structure Formation

The observed grouping of galaxy clusters suggested by current redshift surveys is not immediately understood. Assuming a random distribution of galaxies in the universe, patterns of higher and lower density would naturally be expected. In addition, once the specific density of a region is achieved, gravitational forces act to reinforce the initial density characterization: high density regions become more dense, and lower density regions become less dense. However, large spacial voids are often observed, sometimes reaching distances of several hundred megaparsecs (1pc = 10^{16}m). Using the maximum velocities with which galaxies have been observed to travel (100s of km/s), these distances could not have been traveled during the age of our universe. This result implies that the galaxies could not have formed inside the voids and then moved out. To conclude, we are motivated to look to the first moments of the universe for answers to questions regarding galaxy formation.

In cosmology, the formation of structure on all scales, from planets and stars to galaxies and galaxy clusters, is termed structure formation. The formation of structure is believed to have originated in the first instants of the Big Bang. Quantum mechanical density fluctuations guarantee that, even in these first moments, the distribution of density was not homogeneous. From the standard model of cosmology, it is then predicted that a negative-pressure vacuum energy density forced the infant universe into a phase of rapid, exponential growth. This period of cosmic inflation drove the initial quantum fluctuations to form small regions of overdensity. Observations from the cosmic microwave background and certain redshift surveys provide evidence to suggest that the resulting density fluctuations act as the seed for galaxy cluster formation.

4.1 The Press-Schechter Formalism

A formal picture of how structure formation occurred was not available until thirty years ago when the Press and Schechter (PS) model of spherical collapse was introduced [4]. The PS formulism provides a simple analytical template for generating number counts for structures as a function of mass and redshift. Since the way in which structure is thought to have formed depends on the composition of the universe, the PS machinery is useful in constraining cosmological models.

To begin, the PS model imagines that, within an otherwise homogeneous universe, regions of initial overdensity collapse with spherical symmetry as cosmic expansion takes place [9]. It is assumed that, at any particular time, only structures with a density greater than a specified critical overdensity will have collapsed and virialized. However, since virialized structures are nonlinear density fluctuations, it is not obvious how to handle their evolution. Under the PS theory, it is argued that if the the initial spectrum of these fluctuations was roughly Gaussian, and that the amount of mass contained with a collapsed object is not significantly changed by ignoring the exact nonlinear density evolution, a linearized spherical collapse model is sufficient [9]. Within the linear model, the critical overdensity of an object at virialization is given by [13]:

$$\delta_{sc}^{\nu} \simeq \frac{3(12\pi)^{2/3}}{20}(1 + 0.0123 \log_{10} \Omega_f) \tag{22}$$

where Ω_f is the cosmological parameter expressed as:

$$\Omega_f(z) = \frac{\Omega_m(1+z)^3}{\Omega_m(1+z)^3 + (1-\Omega_m)(1+z)^{(3(1+w_\Lambda))}}. \tag{23}$$

Use of equation (22) assumes a flat universe, $\Omega_m + \Omega_\Lambda = 1$. For the linear growth factor, defined as [14]

$$D(z) = 2.5\Omega_m H_0^2 H(z) \int_z^\infty \frac{(1+z')}{H(z')^3} dz', \tag{24}$$

and Hubble parameter at redshift z given by

$$H(z) = H_0\sqrt{\Omega_m(1+z)^3 + (1-\Omega_m)(1+z)^{(3(1+w_\Lambda))}}, \tag{25}$$

the critical overdensity of an object that virialized at redshift z, has evolved as:

$$\delta_c(z) = \delta_{sc}^{\nu}\frac{D(0)}{D(z)}. \tag{26}$$

In short, $\delta_c(z)$ describes the present-day density contrast, in the linear theory, of a region that underwent spherical collapse and virialized at redshift z. The value of the Hubble constant used in equation (25) is given in Section 2. Under the assumption that the initial spectrum of density fluctuations in the early universe can be described as a Gaussian, the probability of a particular cluster of mass M having an overdensity, at the current time, greater than $\delta_c(z)$ is

$$p(\delta_c(z), M) = \frac{1}{\sqrt{2\pi}\sigma(M)}\int_{\delta_c(z)}^{\infty}\exp(-\delta^2/2\sigma(M)^2)d\delta. \tag{27}$$

The variance $\sigma(M)^2$ found in the Gaussian distribution is normalized to spheres of radius $8h^{-1}$ Mpc through the expression [9]:

$$\sigma(M)^2 = \sigma_8^2\frac{\int_0^{\infty}k^{2+n}T(k)^2|W(kR(M))|^2dk}{\int_0^{\infty}k^{2+n}T(k)^2|W(k8h^{-1}Mpc)|^2dk}. \tag{28}$$

Within the variance equation, σ_8 describes the galaxy fluctuation amplitude and is fit to cosmological data. In this study, we use the five year WMAP result $\sigma_8 = 0.796 \pm 0.036$ [1]. The function $W(x)$, defined as $W(x) = 3(\sin x - x\cos x)/x^3$, ensures that $\sigma(M)^2$ is the variance of the mass distribution in spheres of radius $R(M) = [3M/(4\pi\bar{\rho})]^{1/3}$ by vanishing when $R > R(M)$ ($\bar{\rho}$ is given below). However, as the universe expanded, the distribution of density fluctuations, described by $\sigma(M)^2$, evolved at different rates. Analysis of the power spectrum (energy per unit time as a function of frequency bins) of primordial matter density fluctuations over time has determined that the spectrum may be written as $P(k) = T(k)^2k$, for wavenumber k and the transfer function, defined as [14]:

$$T(k) = \ln(1 + 2.34q)/(2.34q) \times [1 + 3.89q + (16.1q)^2 + (5.46q)^3 + (6.71q)^4]^{-1/4}. \quad (29)$$

In terms of the function Γ [9], where

$$\Gamma = \Omega_m h \exp[-\Omega_b(1 + \sqrt{2h}/\Omega_m)], \quad (30)$$

$q(k)$ is given by

$$q(k) = \frac{k}{\Gamma h Mpc^{-1}}. \quad (31)$$

Within the equation for Γ, Ω_b is the ratio of baryon density to critical density, $\rho_{crit} = (3H^2)/(8\pi G)$. In this paper, we use values from Refs. [11] and assume $\Gamma = 0.2$.

This simple model of structure formation envisions that the first objects to form are small and dense. These small objects merge to form larger bound structures through bottom-up structure formation. Since galaxy clusters are the largest bound structures, describing them using this technique is particularly useful. Through comparison with numerical simulation, the PS formalism developed here has proven to be an excellent analytical model for studying structure formation and predicting galaxy cluster counts. Using the Gaussian probability, equation (27), the number density (number of objects per unit volume) can be expressed as $n(M)$, so that

$$n(M)dM = \frac{\bar{\rho}}{M}\frac{d}{dM}\left(p(\delta_c, M)\right) \quad (32)$$

determines the number density of clusters with mass between M and $M + dM$. The current mean matter density of the universe is $\bar{\rho} = 2.775 \times 10^{11}\Omega_m h^2 M_\odot\ Mpc^{-3}$ [9]. Then, the mass function is given by

$$n(M) = \frac{dN}{dM} = \frac{5}{2}\sqrt{\frac{2}{\pi}}\frac{\overline{\rho}}{M}\frac{d\nu}{dM} exp\left(-\frac{\nu^2}{2}\right). \quad (33)$$

where $\nu = \frac{\delta_c(z)}{\sigma(M)}$ is a function of the cosmology being considered. As cosmology research has improved, Sheth, Mo and Torment (SMT) developed an ellipsoidal collapse model which appears to describe the collapse of overdense regions more precisely as compared with computer simulation. Within the SMT formulism, the mass function is given by [15]

$$n(M) = \frac{dN}{dM} = \sqrt{\frac{2a}{\pi}} c \frac{\overline{\rho}}{M} \frac{d\nu}{dM} \left(1 + \frac{1}{(a\nu^2)^p}\right) exp\left(-\frac{a\nu^2}{2}\right) \tag{34}$$

where $a = 0.707$, $c = 0.322$, $p = 0.3$ are values determined by simulations and, again, $\nu = \frac{\delta_c(z)}{\sigma(M)}$. The difference between the PS and SMT mass functions resides in the parameters a, c, p. In the PS model, $a = 1, c = 0.5$, and $p = 0$. For the current purpose, the SMT mass function will be used.

4.2 Relating Structure Formation Theory with Observations

The structure formation theory just developed generates predictions for the distribution of collapsed objects, such as galaxy clusters, as a function of their masses and redshifts. If telescopes were able to directly measure cluster masses, observations could be compared with theory immediately. However, telescopes typically measure flux and record spectrums from distant clusters. The reconciliation between theoretical predicts and observations come in the form of the $M - T$ relation, relating cluster mass and temperature, and the $L - T$ relation, which relates cluster temperature and luminosity. These relations enable the mass function to predict number counts as a function of the flux limit, f_x, designated by a cluster survey.

The population of a galaxy cluster range from clusters with 50 galaxies to clusters with several thousand galaxies. Between clusters lies the intracluster medium which is thought to be mostly composed of dark matter. A small fraction of this medium takes the form of a hot, baryonic gas that appears to fill the intracluster space homogeneously. Collisions between hydrogen atoms within the gas generate X-rays that can be detected by surveys sensitive to the X-ray spectrum. For the current purpose, the temperature of this baryonic gas will be

referred to as the cluster temperature. In order to arrive at a relationship between the mass of a cluster and temperature, the $M - T$ relation, two assumptions must be implemented. First, the cluster gas is taken to be isothermal. Despite whether or not this is a good model for actual clusters, it is generally thought to not affect the prediction of number counts, which is the current focus. Second, it is assumed that the temperature of the baryonic gas is proportional to the temperature of dark matter particles which dominate the intracluster medium. The temperature of dark matter particles of mass m_D is given by:

$$T_D \equiv \frac{m_D \sigma_D^2}{k_B}, \tag{35}$$

where k_B is Boltzmann's constant and σ_D^2 is the velocity dispersion of the particles. The density of an isothermal, spherical region of dark matter, as a function of distance from the cluster center r, can be written as

$$\rho_D(r) = \frac{\sigma_D^2}{2\pi G r^2}. \tag{36}$$

Next, we define the function $\triangle(z)$ to be the ratio of the density of a spherical object, which has just virialized at redshift z, to the critical density so that $\triangle(z) \equiv \rho_{sc}^v / \rho_{crit}$. An approximation of $\triangle(z)$ was provided in Refs. [16] as a function of $\Omega_f(z)$:

$$\triangle(z) = 18\pi^2 + 82(\Omega_f(z) - 1) - (39(\Omega_f(z) - 1)^2. \tag{37}$$

This expression was created for a flat cosmology with $w_\Lambda = -1$. We assume that any discrepancy generated by $\triangle(z)$ in assuming a cosmological constant (compared to w_Λ as a free parameter) is small. With an expression for $\triangle(z)$ in hand, the mass of a spherical cluster which has virialized at redshift z can be approximated by the mass generated from integrating $\rho_D(z)$ to a given radius so that the mean density equals $\rho_{crit}\triangle(z)$. The result is a scaling relationship between the velocity dispersion of the dark matter particles, σ_D^2 and the cluster mass, M:

$$\sigma_D^2 \sim M^{2/3} H(z)^{2/3} \triangle(z)^{1/3}. \tag{38}$$

The Hubble parameter $H(z)$ is given by equation (25). By extension of the assumption that the cluster temperature, T, was proportional to T_D, we conclude that T scales with σ_D^2. Thus, the cluster temperature and mass are related through the $M - T$ relation:

$$T \sim M^{2/3} H(z)^{2/3} \triangle(z)^{1/3}. \tag{39}$$

The $M - T$ relation used in this study takes the form provided by [17]:

$$T = T_{15} \left(\frac{h}{0.73} \right)^{2/3} \left(\frac{\Omega_m \triangle(z, \Omega_m)}{178 \Omega_f(z)} \right)^{1/3} \left(\frac{M}{10^{15} M_\odot} \right)^{2/3} (1+z), \tag{40}$$

where numerical simulations are used to determine the normalization constant T_{15} (normalized so that masses are in units of 10^{15} solar masses). Some discrepancy exists in the literature as to the precise value of this constant. As a result, we study the sensitivity of our model to the value of this parameter by considering two values: $T_{15} = 6$ keV and 5 keV.

The second piece needed in order to use structure formation formalism to predict number counts (as a function of a specified survey flux limit f_x) is the $L - T$ relation which relates cluster temperature and luminosity. Many complications arise during the implementation of $L - T$ relations cited in the literature [9]. For the current purpose, we will address these complications as they specifically apply to the following formulation. To begin, we adopt the power law $L - T$ relation:

$$L_{0.2-2.4}^{local} = A_6 \left(\frac{T}{6keV} \right)^B \tag{41}$$

found by Markevitch [18] for the 0.2-2.4 keV frequency band. The ROSAT survey quotes flux measurements in the 0.2-2 keV band, so this $L - T$ relation is a practical choice. The expression, fitted for constants $A_6 = (1.71 \pm 0.21) 10^{44}\ h^{-2}$ erg s^{-1} and $B = 2.02 \pm 0.40$, was developed from a group of 35 local clusters with redshift less than 0.1. Next, we consider the cluster luminosity, L, given in terms of the measured flux F through

$$L = 4\pi d_L(\Omega_m, z)^2 F K(z). \tag{42}$$

This expression for the luminosity differs from the one given in equation (16) by the addition of a K-correction, $K(z)$, which converts the luminosity in a specific frequency band in the rest frame (cluster frame) to luminosity in the same band in the lab frame (earth or near earth). The K-correction factor, as a function of cluster temperature T and redshift, takes the form:

$$K(T, z) = \frac{\int_{f_1}^{f_2} df P_T(f)}{\int_{f_1(1+z)}^{f_2(1+z)} df P_T(f)} \tag{43}$$

for a frequency band (f_1, f_2). The rest frame spectral distribution, $P_T(f)$, for a cluster with temperature T, is found to be reasonably represented by a simple power law spectrum

$$P_T(f) \sim f^{-n}, \tag{44}$$

where a power index $n = 0.5$ is implemented to describe the 0.5-2 keV frequency band.

Before our expression for the luminosity can be use to find the cluster temperature T via equation (41), we must be mindful of two features of the $L - T$ relation. First, strong evidence has been collected to suggest that $L - T$ relations evolve in time (as cluster environments change). Second, when using equation (42) to determine luminosity from measured flux, a specified cosmology is assumed through the luminosity distance d_L (see equation (16)). To account for variations in the assumed cosmology used by different studies to generate an evolving $L - T$ relation, we modify equation (41):

$$L_{0.2-2.4}^{local} = A_6 \left(\frac{T}{6keV}\right)^B \frac{d_L(\Omega_m, z)^2}{d_L(1, z)^2} (1+z)^\alpha \tag{45}$$

to explicitly account for the reference cosmology used. The factor $d_L(1, z)^2$ represents a reference cosmology with $\Omega_m = 1$. For the current study, we adopt the following parameter values used by Refs. [9] for equation (45): $\alpha = 0.6$, $A_6 = 1.06$, and $B = 2.02$.

The final element to consider in order to use the structure formation formalism is to account for the fact that telescopes cannot detect arbitrarily dim objects. The selection function is used to determine the probability that a cluster with a given flux will be detected by a particular telescope. This probability is represented as the ratio of the effective sky coverage area, $A_{eff}(f)$, to the geometric survey area, A_{geo}, through

$$P_{sel}(f) = \frac{A_{eff}(f)}{A_{geo}}. \tag{46}$$

Using the theory discussed above, it is now possible to compare calculated and observed number counts. From equation (34), the mass function can be used to generate the distribution of clusters as a function of mass and redshift. The $M - T$ relation, equation (40), converts cluster mass to temperature. The cluster temperature is then transformed to luminosity (and hence flux) through the $L - T$ relation, equation (45). Finally, the details involved with a specific survey study (*i.e.* the flux limit f_x) are accounted for through the selection probability, equation (46).

4.3 Details regarding Comparison of Theory and Observation and Statistical Analysis

The $M-T$ and $L-T$ relations can be combined by substituting equation (40) into equation (45) to obtain the effective $L - M$ relation, $L(M, z)$. However, when models are made to describe this relationship, it is found that at fixed luminosity, there is a spread in the value for the mass. This spread is the result of scatter in both the $M - T$ and $L - T$ relations. Depending on certain variables such as cluster environments and cluster position, one would expect that different masses could emit the same luminosity. Assuming that the scatter is Gaussian, the effective $L-M$ relation, $L(M, z)$, can be modeled as a log normal distribution for the logarithm of the luminosity:

$$P_L(\ln L', z) = \frac{1}{\sqrt{(2\pi\sigma^2_{\ln L})}} \exp\left[\frac{-(\ln(L') - \ln(L(M, z)))^2}{2\sigma^2_{\ln L}}\right]. \tag{47}$$

From analysis of number counts, a value for the upper limit of the dispersion in mass at fixed luminosity is found to be $\sigma_{\ln M} < 0.4$ [19]. The scatter in mass is related to the scatter in luminosity by $\sigma_{\ln M} = \sigma_{\ln L}/p$ where p is a variable related to power index of the effective $L - M$ relation. Assuming both dispersion factors are constant (*i.e.* they do not change with redshift), the luminosity scatter used in equation (48) is taken to be $\sigma_{\ln L} = 0.7$.

To reflect the dependence of the luminosity distribution, the selection probability $P_{sel}(f)$, from equation (46), is multiplied by $P_L(\ln L, z)$ and integrated over the logarithm of the luminosity. The result is the effective selection probability, given by:

$$\tilde{P}_{sel}(M, z) = \int_{\ln L_x(z)}^{\infty} d(\ln L') P_L(\ln L', z) P_{sel}\left(\frac{\exp^{\ln L'}}{4\pi d_L(z)^2}\right), \tag{48}$$

where the argument of $P_{sel}(f)$ is written explicitly in terms of luminosity and luminosity distance. The lower limit of the integral is the luminosity which corresponds to the flux limit of the survey, f_x, through $L_x(z) = 4\pi d_L(z)^2 f_x$.

The differential number of virialzed objects is found by multiplying the number density, $n(M)$, by the comoving volume per steradian:

$$dV(z) = r_s(z)^2 \left(\frac{dr_s(z)}{dz}\right) dz \tag{49}$$

where $r_s(z)$ is the comoving distance from equation (13). From equation (33), we know that within the formalism of structure formation, the number density of objects is written as the mass function $\frac{dN}{dM}$. The theoretical number count is found by integrating the mass function, weighted by $\tilde{P}_{sel}(M, z)$, over mass, and redshift in bins of $\triangle z = 0.1$:

$$N\,(> f_x, z, \Delta z) = A_{geo} \int_{z-\Delta z}^{z+\Delta z} \int_{M(z)}^{+\infty} dz dM r(z)^2 \frac{dr}{dz} \frac{dN}{dM} \tilde{P}_{sel}(M, z). \tag{50}$$

The lower limit on the mass integral, $M(z)$, denotes the lightest cluster at redshift z with flux $f > f_x$, where $f_x = 1.4 \times 10^{-13} ergs^{-1} cm^{-2}$ represents the minimum flux limit for the ROSAT survey. This limit is imposed to ensure that N describes only cluster sized objects. For the ROSAT data, this restriction is equivalent to disregarding clusters with redshift

$z < 0.2$ as $M(0.2) = 1.6 \times 10^{14}\ M_{\odot}$, which is the lower limit of typical cluster mass (clusters range from $10^{14} M_{\odot}$ to $10^{16} M_{\odot}$).

As mentioned previously, this study made use of the ROSAT 400 Square Degree galaxy cluster survey [10]. The clusters were counted in redshift bins of $\triangle z = 0.1$ from $z = 0.25$ to $z = 0.85$. In the cases where a cluster's redshift lied on boundary of two bins, it was accounted for in each adjacent bin. Since the errors included in the ROSAT data were given in terms of the measured flux, for the purpose of this paper, we adopt the strategy of Refs. [9] in estimating the error bars on the number counts. Thus, the error in number count was generated by shifting the measured flux downward by one standard deviation and recording the number of objects which fell below the ROSAT flux limit. A χ^2 statistical analysis was performed by constructing a formula for χ^2, as in equation (18), for the flux limited number counts N, summed over redshift bin:

$$\chi^2 = \sum_{z-bin} \frac{(N_{obs} - N_{th}(\Omega_m, w_\Lambda))}{\sigma^2}, \tag{51}$$

where N_{obs} and N_{th} represent the observed and theoretical counts, and σ is the uncertainties in the measurements as determined from above. Notice that the theoretical number count is a function of Ω_m and w_Λ since these are the parameters which we wish to constrain. Next, the χ^2 equation was minimized to give a best fit of $\chi^2_{min} = 1.71$ for $(\Omega_m, w_\Lambda) = (0.257, -1.30)$. The normalization parameter for the $M - T$ relation assumed in this fit is $T_{15} = 6$ keV.

The observed number counts from the ROSAT survey are shown in Figure 3 along with the theoretical predictions, given by equation (50), for three (Ω_m, w_Λ) cosmological models. The best fit curve is compared to two reference models: a WMAP prior with $(\Omega_m, w_\Lambda) = (0.26, -1)$, and a concordance model with $(\Omega_m, w_\Lambda) = (0.3, -1)$. Within each model we assume the matter density is dominated by cold dark matter which assigns $w_m = 0$.

A χ^2 analysis was also performed for a $M - T$ normalization parameter given by $T_{15} = 5$ keV. The constructed χ^2 equation was minimized to give a best fit of $\chi^2_{min} = 1.59$

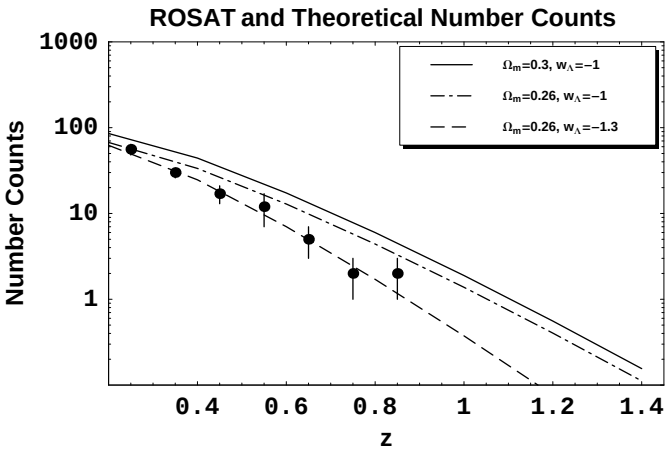

Figure 3: Number counts versus redshift for three curves - the best fit, and two reference models. The error bars associated with the ROSAT observations were estimated by counting the number of clusters that would fall below the survey flux limit if the flux measurements were shifted downward by one standard deviation. This plot is for T15 = 6 keV.

for $(\Omega_m, w_\Lambda) = (0.327, -1.23)$. In Figure 4, the three theoretical curves given for $T_{15} = 6$ keV are depicted again. In comparison with Figure 3, we see that for a given massive object, larger T_{15} essentially adds to the temperature attributed to the object, from which we infer a greater luminosity. This translates into more clusters passing the flux limit, and a larger number count. The effect of lowering T_{15} in Figure 4 is to lower each theoretical curve.

Figures 3 and 4 are useful in illustrating the effect that the equation of state parameter, w_Λ, has on the formation of structure. The negative pressure associated with dark energy has the tendency to increase the the overall gravitational repulsion of substances. Thus, the self-gravity of an overdense region has to work against the expansion in order to collapse. As a result, on large scales structure formation is hindered as w_Λ becomes increasingly negative. Using the clusters observed today as a reference, more negative w_Λ requires the number counts to be greater for larger redshift compared to less negative w_Λ. However, since we already know more negative w_Λ leads to a greater expansion, we expect lower number counts as objects would be dimmer and less would pass the flux limit of the particular

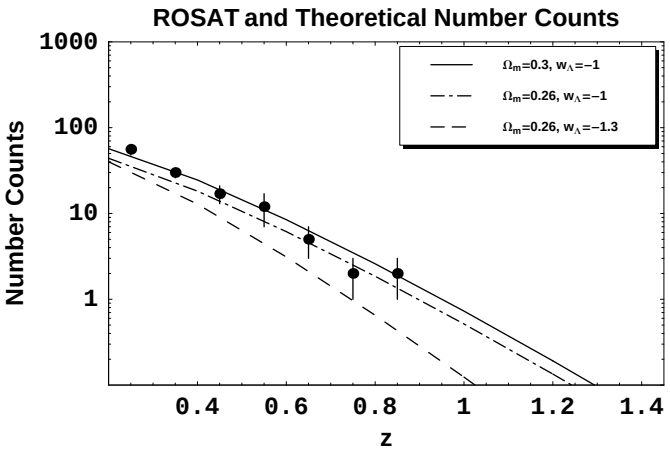

Figure 4: Number counts versus redshift for three curves - the best fit for T15 = 6 keV, and two reference models. The error bars associated with the ROSAT observations were estimated by counting the number of clusters that would fall below the survey flux limit if the flux measurements were shifted downward by one standard deviation. This plot is for T15 = 5 keV.

telescope. This trend can be seen in both Figure 3 and 4 as the cosmological model with $w_\Lambda = -1.3$ under-counts each model with the cosmological constant.

Confidence plots for a (Ω_m, w_Λ) cosmology are created using the same procedure discussed in Section 3.2 for Type Ia SNe. Here, we create plots for the two values of the $M-T$ normalization considered above, $T_{15} = 6$ keV and 5 keV. Figure 5 shows confidence levels for a (Ω_m, w_Λ) cosmology, with $T_{15} = 6$ keV. The best fit value for the matter density found from our structure formation model, $\Omega_m = 0.257$, is consistent with the value given by the five year WMAP results, $\Omega_m = 0.26$ [1]. On the other hand, the best fit value for the dark energy equation of state parameter, $w_\Lambda = -1.3$, is not consistent with cosmological constant $(w_\Lambda = -1)$ that WMAP tends to prefer [1]. Figure 6 shows confidence levels for a (Ω_m, w_Λ) cosmology and $T_{15} = 5$ keV. The same analysis of the best fit values for $T_{15} = 6$ keV applies, except that the matter density, $\Omega_m = 0.327$, is slightly greater than the WMAP value.

Overall, however, despite differences to WMAP preferences, our results are similar to studies conducted by Samushia and Ratra [20], where a dark energy dominated cosmology

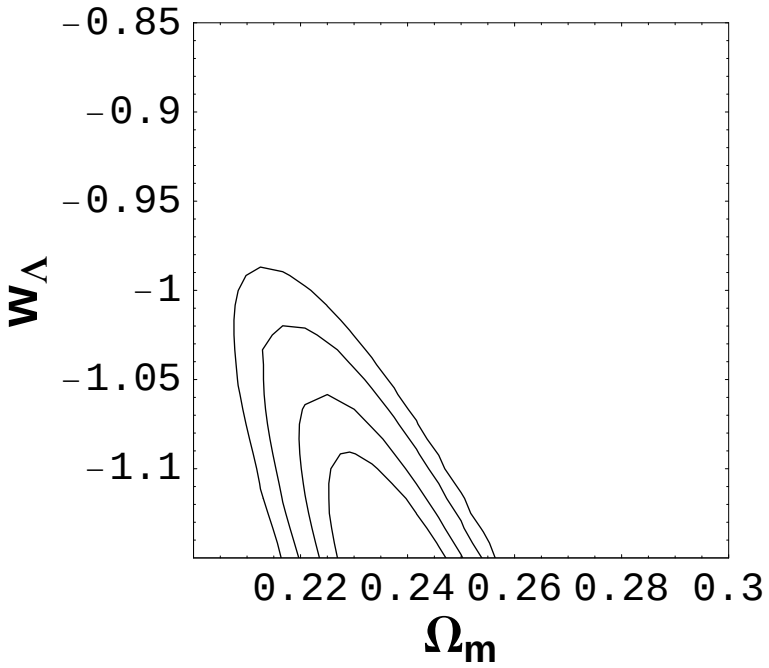

Figure 5: Confidence plots for parameter space with T15 = 6 keV. The lines represent 68%, 80%, 90%, and 95% confidence regions. The best fit is $(\Omega_m, w_\Lambda) = (0.257, -1.30)$.

was constrained using gas mass fraction versus redshift data from X-ray clusters. In the study, the ratio between baryonic and total mass in galaxy clusters is assumed to equal the ratio between the respective cosmological mass density parameters, Ω_b and Ω_m. By comparing measurements of the baryonic mass, a (Ω_m, w_Λ) cosmology is constrained with best fit values of $(\Omega_m, w_\Lambda) = (0.29, -1.2)$ and $(0.27, -1.17)$ for two sources of data. These findings are similar, in particular, to the results found above for $T_{15} = 5$ keV. The trend, seen in Figure 5 and 6, of confidence regions being constrained well for Ω_m, and poorly for w_Λ, is also found by Samushia and Ratra. Though, it should be noted that the confidence regions found by their study occupy more of the parameter space (*i.e.* the confidence ellipses are larger).

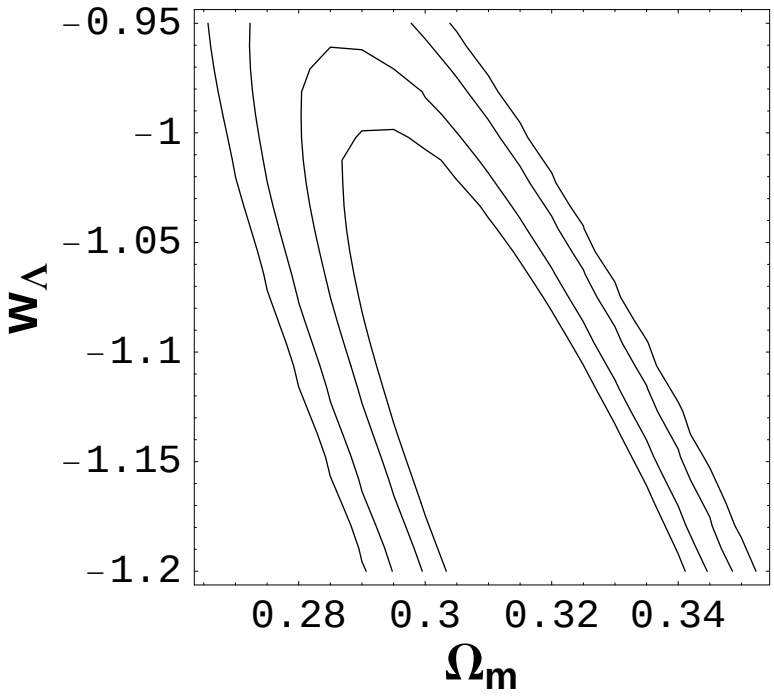

Figure 6: Confidence plots for parameter space with T15 = 5 keV. The lines represent 68%, 80%, 90%, and 95% confidence regions. The best fit is $(\Omega_m, w_\Lambda) = (0.327, -1.23)$.

5 Combining Type Ia Supernovae and Galaxy Cluster Constraints

In current astrophysical studies, consistency checks for cosmological models are accomplished by analyzing sources of data whose dependence on model parameters vary. For example, consistency between data that is sensitive to different combinations of Ω_m and w_Λ may provide confirmation of a dark energy component described by the formulation of general relativity [21]. In this section, the confidence regions of the Type Ia supernovae and the galaxy cluster are superimposed to create a global fit. This is motivated by the fact that SNe and structure formation depend on parameters such as Ω_m and w_Λ differently (see equation (13) and (17) for SNe and equation (25) and (26) for structure). Although a more rigorous analysis could be achieved by combining the statistics of each set of data, for the

purpose of this study, a qualitative comparison is made.

Figures 7 and 8 show confidence plots for the SNe and structure χ^2 analysis for $T_{15} = 6$ keV and 5 keV, respectively; in each case, the SNe contours run diagonally across the space. The global fit for $T_{15} = 6$ keV suggests that the two sources of data are in disagreement as regions of maximum likelihood overlap only in a small region. The combined fit for $T_{15} = 5$ keV shows more agreement between the two data sets. In this case, though a matter density for the combined constraint is larger than the preferred value from WAMP, the cosmological constant, $w_\Lambda = -1$, is within the confined region up to the 68% level for the galaxy data. Overall, however, it is difficult to draw conclusions from these comparisons since the exact value of T_{15} is not known. For both Figure 7 and 8, we can imagine that larger confidence regions for the structure data would provide a modest consistency check. From the cluster study conducted by Samushia and Ratra [20], the (Ω_m, w_Λ) space was constrained in a manner which would suggest general agreement between SNe and cluster data. Thus, the model for structure formation developed in this study should be better analyzed. Sources of systematic error in the structure model developed here are considered in the next section.

6 Systematic Errors in Relating Observations to Mass

There are several sources of uncertainty in the theoretical models which relate measured flux to the mass function. The $L-T$ and $M-T$ relations, given by equations (40) and (45), have errors associated with their assumed power laws. Consequently, this introduces uncertainty in the effective $L-M$ relation. In addition, the values given for the normalization parameters associated with these relations, T_{15} and A_6 respectively, have a nontrivial effect on the prediction of cluster counts. The sensitivity of these counts on the value of T_{15} was shown here. As argued by Refs. [9], the consequences for different values of A_6 is similar to those of T_{15} up to an appreciable percent. Since we have seen that better agreement, between predicted number counts and the $(\Omega_m, w_\Lambda) = (0.26, -1)$ cosmology preferred by WMAP is achieved for lower T_{15}, future work dedicated to studying these effects is well motivated.

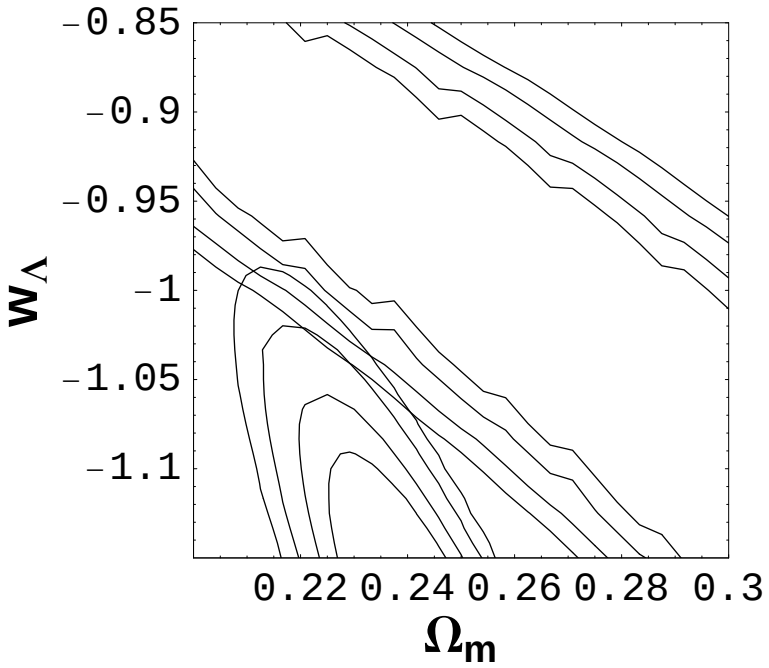

Figure 7: Superimposed confidence plots from Type Ia supernovae and galaxy cluster (with T15 = 6 keV) and data sets. The SNe contours run diagonally across the space. The lines represent 68%, 80%, 90%, and 95% confidence regions for each data set. The best fit for the supernovae data is (Ω_m, w_Λ) = (0.285, -1.05). The best fit for the cluster data is (Ω_m, w_Λ) = (0.257, -1.30).

7 Conclusions and Future Study

In this paper, the basic methods of statistical analysis used in cosmological surveys were studied through a review of observations made by the Supernovae Legacy Survey. Using formulae introduced in our review of cosmology, the theoretical predictions for the magnitude of Type Ia supernovae was compared to observations in order to place constraints on the (Ω_m, w_Λ) parameter space. The best fits obtained from a χ^2 analysis agreed with findings from the SNLS and the five year WMAP results.

We studied analytical models describing structure formation and the comparison of astronomical observations to mass. The predicted number counts of galaxy clusters was

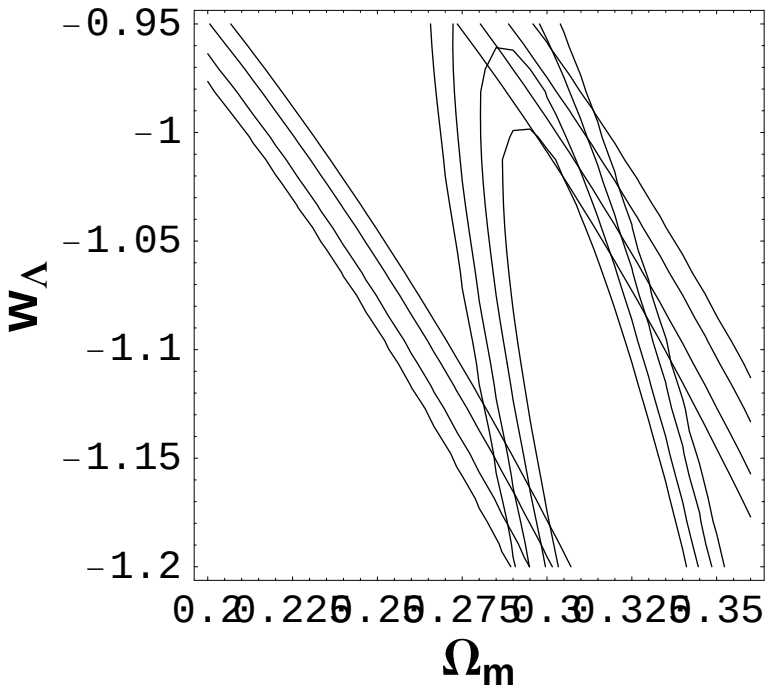

Figure 8: Superimposed confidence plots from Type Ia supernovae and galaxy cluster (with T15 = 5 keV) and data sets. The SNe contours run diagonally across the space. The lines represent 68%, 80%, 90%, and 95% confidence regions for each data set. The best fit for the supernovae data is (Ω_m, w_Λ) = (0.285, -1.05). The best fit for the cluster data is (Ω_m, w_Λ) = (0.327, -1.23).

then compared to the observed counts from the ROSAT X-ray survey. A χ^2 analysis for two values of T_{15} revealed two (Ω_m, w_Λ) fits that roughly agree with WMAP for the value of Ω_m, but not for w_Λ. We cited the findings of Samushia and Ratra where similar results for (Ω_m, w_Λ) were found using a different X-ray cluster approach. In addition, it was shown that best agreement between predicted number counts and the $(\Omega_m, w_\Lambda) = (0.26, -1)$ cosmology preferred by WMAP occurs for lower T_{15}. On account of this, and other sources of theoretical uncertainty, further attention to the analytical model developed in this paper is deserved.

In a broad sense, the formalism developed in this study provides a basis for future work

that would be as educational as it would be useful. The ability of Type Ia supernovae and flux limited cluster counts to constrain other cosmological parameters could be easily tested using the model described above. Results could be used as consistency checks for other sources of data such as the CMB described by WMAP. Also, the theoretical uncertainties in certain features of the structure formation model could be examined by studying χ^2 fits for different parameter values.

References

[1] E. Komatsu *et al.*, *Five-Year Wilkinson Microwave Anisotropy Probe (WMAP) Observations: Cosmological Interpretation*, (2008), [arXiv.org:0803.0547].

[2] S. Perlmutter *et al.*, *Measurements of Omega and Lambda from 42 High-Redshift Supernovae*, *The Astrophysical Journal*, 517, 565, (1999), [astro-ph/9812133].

[3] J. Dunkley *et al.*, *Five-Year Wilkinson Microwave Anisotropy Probe (WMAP) Observations: Likelihoods and Parameters from the WMAP data*, (2008), [arXiv.org:0803.0586].

[4] W. Press and P. Schechter *Formation of Galaxies and Clusters of Galaxies by Self-Similar Gravitational Condensation*, *The Astrophysical Journal*, 187, 425-438, (1974).

[5] P. Astier *et al.*, *The Supernova Legacy Survey: Measurement of Omega_M, Omega_Lambda and w from the First Year Data Set*, 447, 31, (2006), [astro-ph/0510447v1].

[6] V. Springel *et al.*, *The large-scale structure of the Universe*, *Nature*, 440, 1137, (2006), [astro-ph/0604561].

[7] A. R. Wetzel *el al.*, *The Clustering of Massive Halos*, *The Astrophysical Journal*, 656, 139, (2007), [astro-ph/0606699].

[8] A. Fuzfa *et al.*, *Some impacts of quintessence models on cosmic structure formation*, (2006), [astro-ph/0611284].

[9] J. Erlich, B. Glover, N. Weiner, *Sensitivity and Insensitivity of Galaxy Cluster Surveys to New Physics*, (2007), [arXiv:0709.3442v2].

[10] R. A. Burenin *et al.*, *The 400 square degrees ROSAT PSPC galaxy cluster survey: Catalog and statistical calibration*, (2006), [astro-ph/0610739].

[11] D. N. Spergel *et al.*, *Wilkinson Microwave Anisotropy Probe (WMAP) Three Year Results: Implications for Cosmology*, *APJS*, 170, 377, (2007), [astro-ph/0603449].

[12] J. Erlich and C. Grojean, *Supernovae as a probe of particle physics and cosmology*, *Physical Review D*, 65, (2002).

[13] T. Kitayama and Y. Suto, *Semi-analytic predictions for statistical properties of X-ray clusters of galaxies in cold dark matter universes*, *The Astrophysical Journal*, 469, 480, (1996), [astro-ph/9604141].

[14] S. Borgani *et al.*, *Cosmological Constraints from the ROSAT Deep Cluster Survey*, (1999), [astro-ph/9901017].

[15] R. Sheth *et al.*, *Ellipsoidal collapse and an improved model for the number and spatial distribution of dark matter haloes*, (2001), [astro-ph/9907024].

[16] G. Bryan and M. Norman, *Statistical Properties of X-ray Clusters: Analytic and Numerical Comparisons*, *The Astrophysical Journal*, 495, 80, (1998) [astro-ph/9710107].

[17] S. C. Vauclair *et al. The XMM–NEWTON Omega Project: II.Cosmological implications from the high redshift L-T relation of X-ray clusters*, *Astronomy and Astrophysics*, 412, L37, (2003), [astro-ph/0311381].

[18] Maxim Markevitch, *The Lx-T Relation and Temperature Function for Nearby Clusters Revisited*, *The Astrophysical Journal*, 504, 27, (1998) [astro-ph/9802059].

[19] R. Stanek *el al.*, *The X-Ray Luminosity–Mass Relation for Local Clusters of Galaxies*, *The Astrophysical Journal*, 648, 956, (2006), [astro-ph/0602324].

[20] L. Samushia, B. Ratra, *Constraints on Dark Energy from Galaxy Cluster Gas Mass Fraction versus Redshift data*, (2008), [arXiv.org:0803.3775].

[21] S. Wang, *et al.*, *Is Modified Gravity Required by Observations? An Empirical Consistency Test of Dark Energy Models*, *Physical Review D*, 76, (2007), [PhysRevD.76.063503].